Summary of Experimental Core Turbulence Characteristics in OH and ECRH T-10 Tokamak Plasmas

V.A. Vershkov, L.G. Eliseev, S.A. Grashin. A.V. Melnikov, D.A. Shelukhin, S.V. Soldatov, A.O. Urazbaev and T-10 team

Nuclear Fusion Institute, Russian Research Center "Kurchatov Institute"
123182, Kurchatov Sq. 1, Moscow, Russia

E-mail: Vershkov@nfi.kiae.ru

Abstract. This report summarizes the results of experimental turbulence investigation, carried out at T-10 more then ten years. The turbulence characteristics were investigated by means of correlation reflectometry, multipin Langmuir probes and Heavy Ion Beam Probe diagnostics. The OH and ECRH discharges show the distinct transition from the core turbulence, having complex spectral structure, to the unstructured one at the periphery. The core turbulence includes the "Broad Band" (BB), "Quasi-Coherent" (QC) features, arising due to the excitation of rational surfaces with high poloidal m-numbers, "Low Frequency" near zero, and the special oscillations at 20 – 30 kHz. All experimentally measured properties of Low Frequency and High Frequency QC are in good agreement with behavior of the linear increments of ITG/DTEM instabilities. Significant local decrease of the turbulence amplitude and coherency were observed near q=1 radius 5 – 15 ms. after ECRH switch off. These evidenced the ITB formation due to turbulence stabilization near rational q=1 surface with low magnetic shear

1. Introduction

The investigation of the physical mechanisms of small-scale tokamak turbulence draw significant attention last decade, because the real control of the anomalous turbulent transport in "advanced tokamak" regimes became an important issue, which suggest the clear understanding of both the physical turbulence mechanisms and the conditions of its stabilisation. This paper summarizes the results of turbulence investigation with correlation reflectometry (CR), Multipine Langmuir Probes (MLP) and Heavy Ion Beam Probe (HIBP) in T-10 tokamak [1-10]. The main goal of the experimental program was identification of the physical mechanisms of the plasma turbulence. The three instabilities are considered now as the cause of the core anomalous transport. These are Ion Temperature Gradient (ITG) [11], Dissipative Trapped Electron Mode (DTEM) [11] and Electron Temperature Gradient (ETG) [12]. The edge plasma turbulence may be caused by Drift Resistive Interchange instability DRI [13]. The T-10 diagnostic capabilities enable to investigate three of these instabilities, with the exception of ETG due to low sensitivity for the wavelengths less then 1 cm. In such approach stability is determined by local plasma parameters and the fluctuations are excited by the temperature gradients, associated with the values of the heat fluxes, and stabilized by the steep density gradients. Unfortunately the experimental turbulence spectra may have footprints of the physical turbulence mechanisms only in linear, or quasi-linear stage, but these features should disappear in the strong non-linear turbulence stage. So in order to reveal the physical turbulence mechanisms the experimental conditions were varied from marginally stable up to strong turbulence cases. To study this approach, the turbulence characteristics were investigated over the whole plasma column in wide range of parameters from the high confinement Ohmic discharge with peaked density up to ECRH 1.4 MW heated discharges with flat density profiles and degraded confinement. The investigations of turbulence physics supposed the determination of the temporal and spatial turbulence characteristics of density and potential fluctuations. Thus a set of diagnostics was used, capable of measuring poloidal, radial and long distance toroidal turbulence properties, including (CR), (MLP), (HIBP) and High Frequency Magnetic Probe (HFMP). The possibility of direct comparison of the data of different diagnostics in equal plasma conditions greatly enhanced the reliability of the results. The significant restrictions of reflectometry are widely discussed in literature. So important topic of the investigations was the simulation of the electromagnetic wave reflection from turbulent plasma in real T-10 geometry with 2D full-wave code. Such simulations enable to understand clearly the limitations of reflectometry in measuring of the short waves and radial correlations, which greatly enhanced its reliability. The current tokamak experiments show a number of different physical mechanisms of the turbulence transport suppression. These are the velocity shear stabilization [14], important role of the low m/n rational surfaces [15] and s - α stabilization [16]. The characteristics of the turbulence in core e-ITB were investigated in T-10 experiments. In difference to the local approach, a non-local plasma response to the fast perturbations seen in many experiments [17] was investigated in the dynamic turbulence evolution after fast edge cooling and at the start phase of ECRH were also investigated

2. Experimental set up

The locations of (CR) antennas, MLP and T-10 limiters are shown in Fig.1. T-10 has circular plasma cross-section with the major and the minor radius of 1.5 and 0.3 m. respectively. The graphite permanent circular and movable rail limiters at radii 0.33 and 0.3 m defined the plasma column. The typical plasma current vary from 100 to 300 kA, toroidal magnetic field from 1.5 to 2.5 T and mean plasma density from 1 to 5×10^{19} m^{-3}. The CR [6] and MLP [4] were able to measure poloidal and radial turbulence characteristics. The CR had two antenna arrays, probing the plasma from the Low Field Side (LFS) and High Field Side (HFS). All antennas were aligned to the centre of the plasma column. It was possible to probe the plasma simultaneously from both the HFS and the LFS in order to measure the poloidal asymmetry of the turbulence and long distance poloidal and toroidal correlations [5,6]. The reflection of O-mode was used in the frequency range 22-78 GHz, was covered with the four independent systems. Up to three reflectometers have been used in a single discharge, enabling wide range of the radial correlation measurements. The amplitude (A) and the phase (φ) of the reflected electric field vector fluctuations were decomposed by a quadrature detector in imaginary ($U_1=A\times\sin\varphi$) and real ($U_2= A\times\cos\varphi$) parts. Thus for each reflectometry channel two signals were recorded. In order to make poloidal correlation measurements, two channels poloidally separated were synchronously sampled using 4 ADCs. All signal processing was made in complex form. The time interval of interest was divided in sub-intervals and in each sub-interval a complex FFT was applied. The sub-spectra were then averaged to obtain two global complex spectra (one for each channel). At the same time the cross-spectrum was taken between the two channels. This consists of the cross-phase and coherency spectra, normalized over the spectra of the two channels. Auto and cross-correlation of the two channels were also performed. The available 8 ADCs with the sampling rate 800 kHz enable to record simultaneously the signals from four arbitrary antennas, which gave possibilities for simultaneous poloidal (short distance between LFS array and long distance between LFS/HFS arrays) and radial correlations. The maximal resolved frequency was

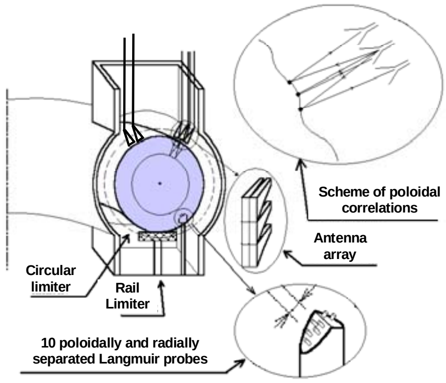

FIG. 1. Correlation reflectometer and Langmuir probe set up

400 kHz. The radial and poloidal CR locality were specially investigated by simulations of the wave reflection from turbulent plasma with 2D full-wave "Planar RτH analyser" code [18] in real T-10 geometry and was checked in special experiments by direct comparison with MLP at the edge. It was found that for all radii sensitivity do not decrease significantly for the wave numbers $k < 3$, which is typical for T-10. The numerical simulations and analytical estimations showed that reflectometry is able to measure the radial correlations of the turbulence. The estimation of the turbulence velocity may be found from the ratio of the antennas reflection spots separation dx and the time delay of the two reflected signals Δt as $V = dx/\Delta t$, provided that perturbations do not decay rapidly. The good agreement of the velocities and amplitude spectra measured with CR and MLP at the plasma edge prove the reliability of reflectometry. It should be stressed that due to the long extension of perturbation along the magnetic field line, the measured velocity principally always has poloidal and toroidal contributions. The MLP was equipped with the six poloidal and three radial pines. The probe was moved radially from discharge to discharge from the wall up to 1.5 cm. into the region with closed magnetic lines. The ion saturation current or the floating potential from any six pines can be recorded simultaneously in one discharge, also enabling simultaneous poloidal and radial correlations. The HIBP [8] diagnostic was situated in the port, separated 90 degrees toroidally from reflectometry port. The measurements were done with Tl^+ beam with energies 200-240 keV. The radial size of the sample volume was estimated as ~1.5cm. The sampling rate was 10 μ. HIBP and reflectometry were able to operate simultaneously in the same radial zone $0.86<\boldsymbol{r}/\boldsymbol{a}<1$. At the plasma edge ($0.95<\boldsymbol{r}/\boldsymbol{a}<1$) they overlapped with Langmuir probes.

3. Radial variations and the boundaries of the core turbulence

The OH and ECRH discharges show the distinct transition from the core turbulence to the SOL. Figure 2 presents the results of the complex poloidal correlation analysis. The typical amplitude Fourier spectrum of the first signal (top traces) and cross-spectra between two signals, including the poloidal cross-phase (middle) and coherency (bottom) are shown for the SOL, central and edge core regions. A pronounce difference is clearly seen. The core turbulence rotates in electron diamagnetic drift direction and has complex structure. It includes the background "Broad Band" (BB) fluctuation, High Frequency (HF) and Low Frequency (LF) "Quasi-Coherent" (QC) spectral maxima typically at frequencies 70-120 and 150-250 kHz respectively and "Low Frequency" (LF) peak at zero frequency. The special fluctuations at 20 – 30 kHz (not shown in Fig. 2) are also seen at low densities in core regions [8, 5]. So it is possible to distinguish five components in the core spectrum. The core edge turbulence retains only LF QC, while HF QC vanishes. In difference to the core, SOL fluctuations have a single spectral maximum at zero frequency and turbulence rotation changes the sign to the ion diamagnetic drift direction. Thus the turbulence velocity shear layer occurs at some radius. The MLP measurements at the edge show that shear layer is determined by the reversal of the radial electric field. The reversal of the radial electric field in that case is naturally connected with the dramatic change of the electron-ion balance due to the parallel escape of the electrons to the limiter. In fact it was observed for Ohmic discharges in different conditions. It was also seen that poloidal and radial correlation lengths are reduced in velocity shear zone. The experimental radial positions of the velocity shear layer for 1.4 MW ECRH discharges with plasma currents 150, 250 and 305 kA are shown in Fig. 3 with the arrows. It is clearly seen that the velocity shear layers in ECRH are not connected with the limiter, but they are shifted well inside the plasma. In this case the relative change of the electron-ion balance can be caused by the change of turbulence type from core ITG/TEM to the edge DRI. The calculated radial dependencies of the growth rates

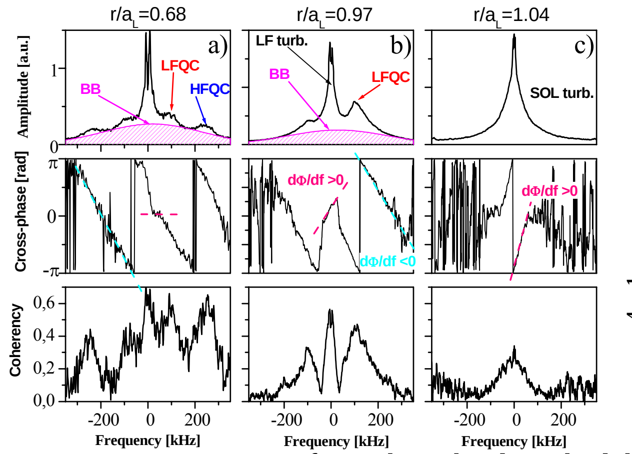

FIG. 2.Fourier spectra of signal amplitude, poloidal cross-phase and coherency at different plasma radii

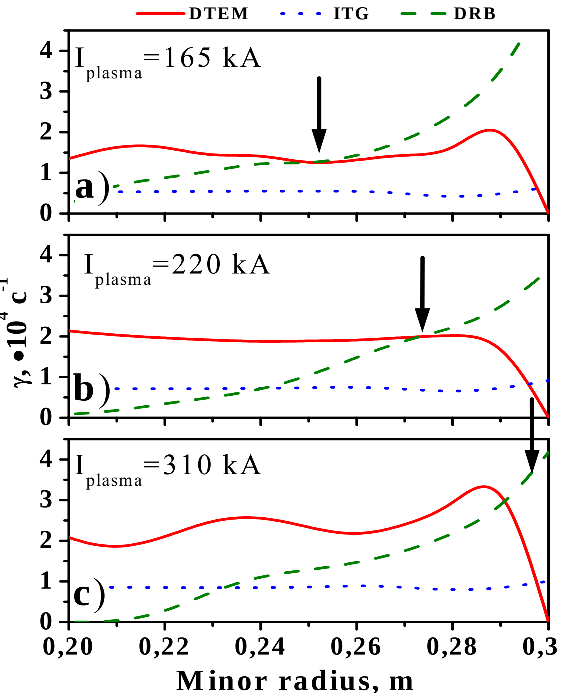

FIG. 3. Radial dependencies of ITG, DTEM and DRB instabilities growth rates

for all three instabilities [11,13] are presented in Fig.4 by the different lines. One can see a good agreement of the experimental position of the shear layer with the regions where DRI become dominant. The validity of such approach is supported by the fact that it naturally explains the experimental increases of the shift to the plasma center with the decrease of the current. So it can be concluded that in L mode the plasma edge is dominated by DRI, while core is connected with other instability types. These experiments clearly showed the plasma region, where the core turbulence is dominant, which is the topic of the present paper.

4. Characterization of turbulence types by radial correlations

The measurements of the radial correlation properties appeared to be very informative in characterization of different fluctuation types. Two quantities are obtained in such measurements: the radial correlation length and the variation of the time delay with the radial separation. The radial correlation and time delay curves were obtained by plotting the maximal value of the cross-correlation function and its time shift. These data are presented in Fig. 4 for three turbulence types. The left column corresponds to LF, the middle one for the LF QC and the right one for the BB turbulence. The cross-correlation characteristics for each type were obtained by means of initial filtering of the raw data. In this way for LF, LF QC and BB the frequencies from 10 to 30 kHz (without special oscillations at 15 – 30 kHz), 80 – 120 kHz and 150 – 400 kHz were filtered respectively. It is clearly seen that BB has the shortest correlation length of 0.5 cm with zero time delay. In fact BB has practically zero poloidal coherency and one can regard it as the noise background. But, firstly, in some Ohmic discharges a low, but definite poloidal coherency was observed with reflectometry. In such cases

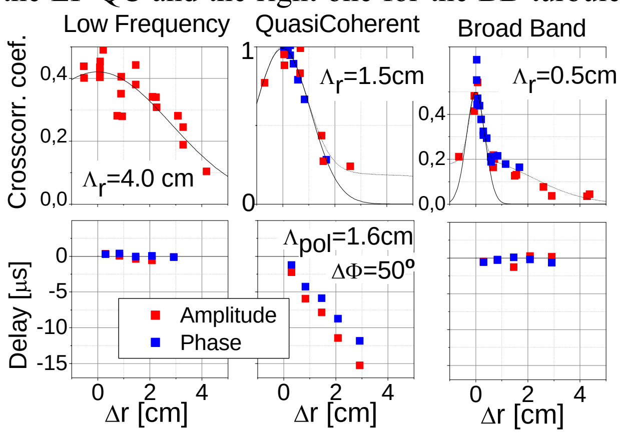

FIG. 4. Turbulence types characterization by radial correlations at ρ=0.5

the velocity of BB were the same as for the QC fluctuations. Secondly, the Langmuir probe spectra have similar BB feature, but in this case locality is high, noise level is low and poloidal and radial coherency are definite. So BB should be regarded as a real turbulence. It may arise due to the stochastic excitation of a single mode with high poloidal m number. In difference to BB, the radial correlation length of LF QC turbulence is the three times longer and the time delay is pronounced and increases with radial separation. This result can be formally treated as the radial propagation of QC with the velocity 2.3×10^3 m/s in addition to poloidal velocity 2.8×10^3 m/s. Nevertheless the other hypothesis seems more real. It explains the observed phase shift of QC by rotation of helical “fingers”, inclined to the radial direction, which arise in 3D gyrokinetic simulations due to the toroidal coupling of several mode with close poloidal m numbers [19]. This hypothesis consistent with the longer radial correlation length and estimated angle 50^0 of the “fingers” with respect to the radial direction is in good agreement with the gyrokinetic simulations. The LF has the longest correlation length about 4 cm. with zero time delay. These properties are similar to “streamers”, which arise in theory [20].

5. Specific modes in frequency range “15 - 30” kHz

The nearly monochromatic oscillations are typically observed in the frequency range 15 – 30 kHz with CR, MLP, HIBP and HFMP [1,8,10]. Similar phenomena had been observed, firstly in TEXT [21] and T-10 [1] and, recently in DIII-D, [22], CHS [23] and ASDEX-U [24]. They have a number of specific characteristics, which make them very different from other types of fluctuations. The typical Fourier spectra of the secondary current and potential fluctuations obtained with HIBP diagnostic presented in the Fig. 5. One can see that relative level of the mode in potential is much higher than that in the density. This property is also confirmed by the MLP. The estimated ratio of $\delta\varphi\times e/Te$ and $\delta n/\langle n\rangle$ is near to 10, in difference with one for QC and 1.7 for BB [6]. The poloidal phase shift of the density fluctuations for this mode was measured by MLP with separation 1.75 cm. and with CR with poloidal angle separation of 5^0 and 55^0. In all cases the values of cross-correlation were high and the cross-phase were equal to zero. This means, that this mode has global structure and zero poloidal m number. The reflectometry radial correlations show significant time delay, which rises with radial separation, as shown in Fig. 6. The estimated radial mode extension from the amplitude variation and the phase shift is about 4 – 8 cm. The experimental data show that the mode significantly influenced the total turbulence level. Figure 7 present the spectra of the phase of reflected wave and the fluctuation of the total turbulence level in the

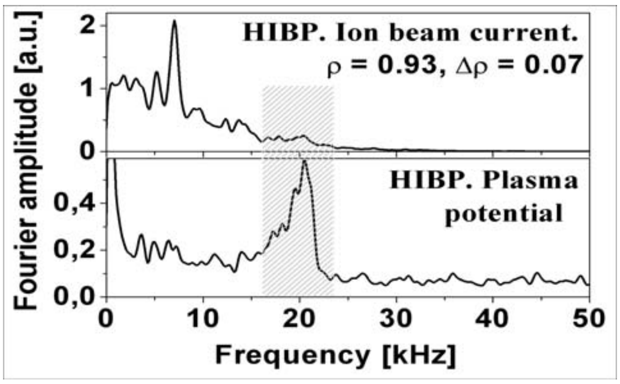

FIG. 5. HIBP. Spectral representation of the beam secondary current and potential signals at ρ=0.93.

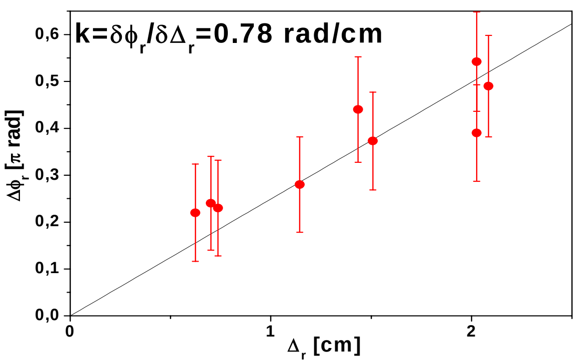

FIG.6. Reflectometry. Phase delay between density fluctuations at close radii as a function of Δr.

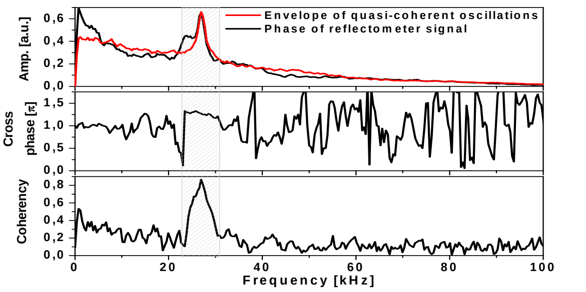

FIG.7. Reflectometry. Correlation between specific mode with m=0 and amplitude of fluctuations in the phase of reflected signal.

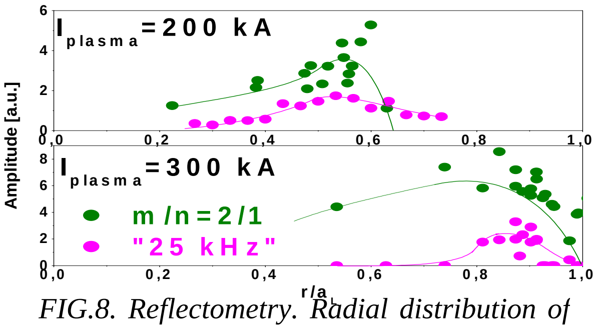

FIG.8. Reflectometry. Radial distribution of the specific mode with m=0 (f=25 kHz) and MHD m/n=2/1 density oscillations.

frequency range 150 – 400 kHz and their cross-correlation. Clearly seen that about 10% of the total turbulence level oscillates with the mode frequency and the coherency is near to 0.9. All these properties are similar to the predicted by theory “zonal flows” [25]. The frequency of the mode rises as $T_e^{1/2}$ and its value is near to the $C_s/2pR$, predicted for the Geodesic Acoustic Modes [26], which are the branch of “zonal flows” [25]. It is important to point out significant coherency and constant cross-phase in Fig. 7 also at frequencies up to zero. This may be indication of the predicted by theory “zonal flows” with the frequencies near zero. Unfortunately up to now in T-10 no clear indications of plasma flows with frequencies about 1 kHz, as were observed in CHS [23] and ASDEX-U [24]. It is important to present also a number of experimental T-10 data, which seems not consistent with the simple theory of “zonal flows”. The case is that the amplitude of the mode strongly localized near rational surfaces, especially q=2. Figure 8 shows the radial distribution of the mode and of the MHD m/n=2/1 density oscillations for two discharges with different q(a) value. Clearly seen that mode located near q=2 region and shifted outward with the decrease of q(a). Moreover, the mode has finite structure inside m/n=2/1 island, as it shown in Fig. 9 [27]. Both the mode satellites and island width and position were measured with reflectometry. Clearly seen that there are three components 20, 23 and 26 kHz within the island. The important feature is presence of some magnetic field fluctuation, associated with that mode, which had been reported also in TEXT [21]. It is observed only in some discharges. In difference to poloidal m number 12 in [21,22] from the density perturbations, m=0 was measured in T-10 with CR and MLP. The last peculiarity of the mode in T-10 is that it is observed with reflectometry only at the local densities lower then 2×10^{19} m^{-3}. In principle this may be indication of strong damping of “zonal flows” with collisionality discussed in theory.

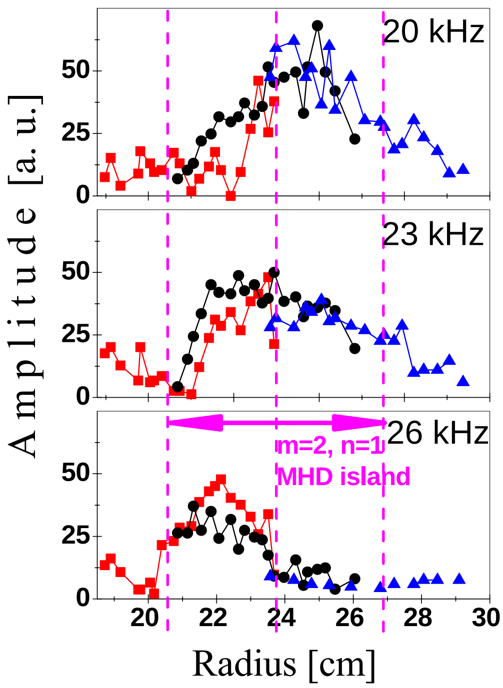

FIG.9. Reflectometry. Detailed analysis of the specific modes with m=0 in the vicinity of q=2 position.

6. Characterization of LF and HF Quasi-Coherent fluctuations

The typical core amplitude spectrum of fluctuations is shown in Fig. 2 and exhibits two spectral maxima. The LF QC usually observed at 70-120 and HF QC at 150-250 kHz. The strong difference of their spatial structure is proved by the data in Fig. 10. A single maximum of HF QC turbulence was observed at frequency of 200 kHz at LFS,

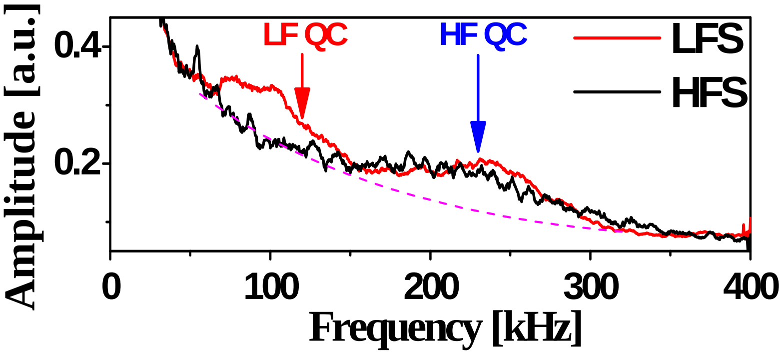

FIG.10. Reflectometry. Spectral characteristics of LF QC and HF QC modes at LFS and HFS.

while both LF and HF maxima clearly seen at LFS. The radial scan of k×ρ_i values for both QC types together with the linear growth rates of ITG [11], DTEM [11] and BRI [13] instabilities are presented in Fig. 11 respectively. Experiment showed only LF QC at the core edge (0.8 <r/a<1), where only ITG is unstable, while in the plasma core both LF and HF QC maxima are seen in accordance with the increments of ITG and DTEM. It should be stressed that the appearance of HF QC at r/a=0.8 just coincides with the rise of DTEM growth rate. It is important that in core plasma the k×ρ_i values approach 0.3 for LF QC and 0.7 for HF QC as are expected from theoretical estimations for ITG and DTEM. The radial distributions of the amplitudes of both modes, values of linear growth rates and η_i are shown in Fig. 12 for the two phases of Ohmic discharge. The data of the left column was taken during the strong working gas influx at the density build up phase. The measured density profile is broad in this case. The right column corresponds to the stationary discharge conditions with more peaked density profile. The radial distribution of the modes showed that LF QC exists near centre and at periphery. This is in good agreement with the regions of maximal η_i values. In difference HF QC is maximal at a/2 at maximal population of the trapped electrons and, thus, DTEM increment. Figure 12 clearly show that after evolving of the discharge to the stationary conditions with more peaked density the LF QC is stabilized from 12 to 17.5 cm. This behavior again is consistent with stabilization of ITG by the density gradient. This is in agreement with the decrease of η_i and growth rate of ITG. At the same time the amplitude of HF QC is increased in accordance with DTEM growth rate increases. So both, the radial

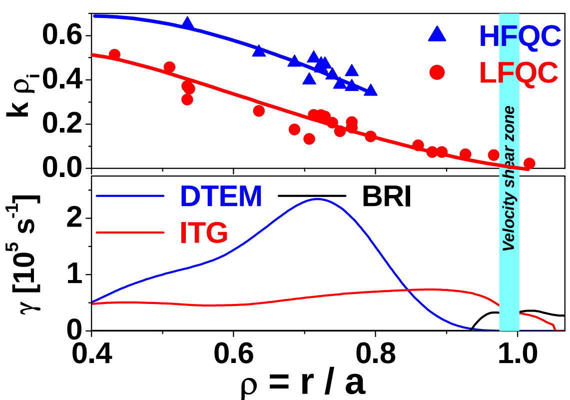

FIG.11. Reflectometry. Radial distribution of HFQC and LFQC modes in comparison with radial profiles of linear increments calculated for DTEM, ITG, and BRI instabilities.

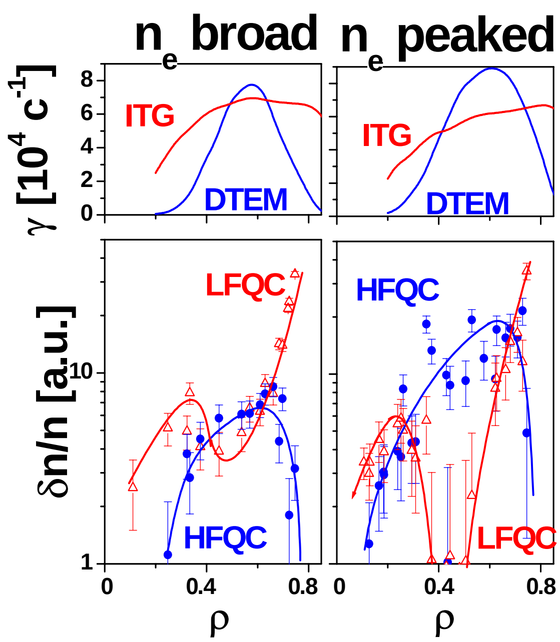

FIG.12. Radial profiles of linear increments calculated for DTEM and ITG instabilities in comparison with experimental radial distribution for HFQC and LFQC modes amplitude.

behavior and reaction to the density peaking, are consistent with the hypothesis that the origin of LF and HF QC are ITG and DTEM instabilities. This correspondence is also supported by the values of $k \times \rho_i = 0.3$ for LF QC in core regions of discharges with different toroidal magnetic field strength from 1.5 to 2.5 T in T-10. Extremely wide scan was obtained by comparison of T-10, TEXTOR and FTU results in [10]. For r=a/2 all values were near to 0.3 in the wide range of magnetic field up to 8 T, as predicted for ITG instability.

7. Behavior of turbulence in OH and central ECRH discharges with different densities

The special series of experiments with average density variation in OH and ECR heated discharges were carried out. The evolution of the turbulence amplitude spectra were monitored at r=a/2 by means of variation of the launched wave frequency. The results of this experiment are shown in Fig. 13. The left figures correspond to the low and right one to the high densities. The top figures present ohmic and the bottom ECR heated discharges. The three distinct trends are clearly seen. The first is the obvious evolution of he turbulence from LF QC at low to the HF QC at high densities. This change of turbulence type is in line with the general tendency always observed in T-10: LF QC always observed in the plasma regions and in discharges with high particle convective fluxes. It occurs at plasma edge, under strong gas puff at density build up phase and during strong recycling during ECRH, as will be shown below. The HF QC, vice versa, typical for the regions with low particle convection. This is consistent with dominant LF QC at low density, where plasma transparent for neutrals and convection is high. At the high density neutrals do not penetrate, convection is low and HF QC is dominant. The second trend is a factor of two rise of the total turbulence level in 1 MW ECRH and degraded confinement. The third trend is the strong decrease of the QC maxima contrast with increase of the heating power and turbulence level. This may be explained by the turbulence transition from the linear, or quasi-linear phase, where the features of the linear instability still exist, to the strong non-linear phase, where all linear features disappear. One of the possible non-linear mechanisms is the increase of the amplitude of the "zonal flows" at high turbulence level, which destroy the toroidal mode coupling, responsible for QC formation. As it is seen in non-linear case turbulence spectra became similar and it is impossible to deduce the physical mechanism of instability. The ECR heated discharges with different average density give the unique possibility to follow the turbulence wavelength dependence either on ρ_I or on ρ_S. This can be done because Te is strongly decreases with density rise, while Ti only rises. Thus the Te /Ti ratio decreases from 7 up to 1.5. The analysis of the turbulence data again prove that even in such conditions $k \times \rho_i = 0.3$ still valid, while $k \times \rho_s$ vary from 0.8 to 0.4 for LH QC. So we can conclude that the value of electron temperature do not determine wavelength of the LH QC turbulence.

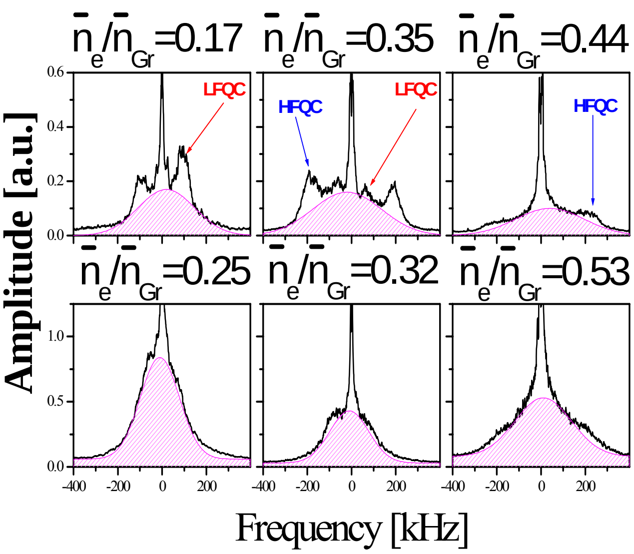

FIG.13. Reflectometry. Spectral characteristics of turbulence versus plasma density and ECR heating.

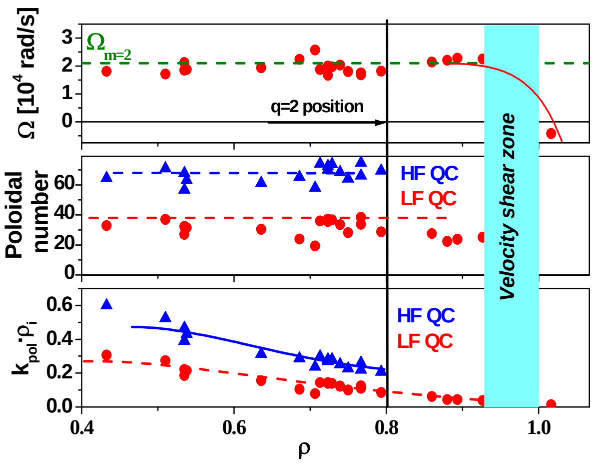

FIG.14. Reflectometry. Angular velocity, poloidal mode number and $k_\perp \times \rho_I$ for discharge with low q value at the periphery

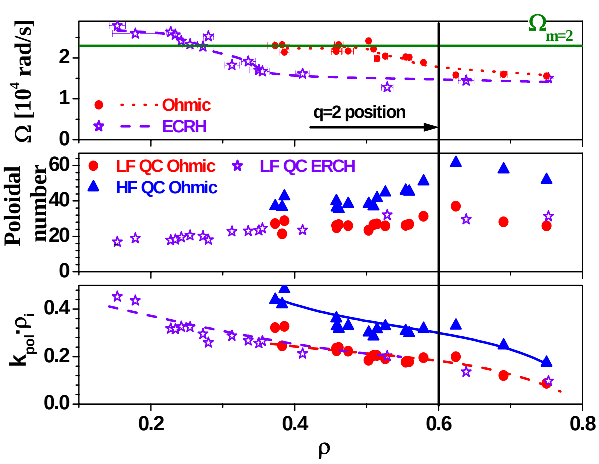

FIG.15. Reflectometry. Angular velocity, poloidal mode number and $k_\perp \times \rho_I$ for discharge with low q value at the periphery

8. Turbulence rotation

The evidence of some interaction between the plasma layers, which are radially away of each other may be found in Fig. 14. It presents the radial dependence of turbulence parameters in the ohmic discharge with current 300 kA, magnetic field 2.42 T and average density 4×10^{19} m^{-3}. Figure 14a shows the radial variation of the angular turbulence rotation and Fig. 14b the poloidal m numbers of the LF and HF QC turbulence. One can see that the angular turbulence rotation is remarkably constant over the whole plasma radii. Moreover it coincides with that of MHD m=2 island rotation. Figure 14b shows that poloidal m numbers are also constant. Thus the turbulence rotates over all radii like rigid body with the angular velocity of m=2. It should be stressed that rigid body rotation together with the m=2 mode is the most general feature. It is clearly seen that this constrain breaks only at the edge velocity shear layer. The slightly different behavior occurs at higher q(a) values, as shown in Fig. 15. The edge outside q=2 radius rotates slower, while inside q=2 turbulence rotation increases again just up to the rotation of m/n=2/1. This may be explained by the decrease of the m/n=2/1 amplitude at high q discharge. In this case it can't controlled the whole plasma, but only core region inside q=2. Thus the experimental data gives possiblity to suggest that the global interaction exists, which forced all fluctuations to rotate together with MHD m=2 island. The constancy of poloidal m numbers naturally leads to the short wavelength gyrobohm diffusion in the centre with $k_{pol}\times\rho_i$ =0.3 and Bohm diffusion at the edge with $k_{pol}\times\rho_i$ =0.05 (Fig. 14c). It is important to note that rigid body rotation easily breaks under strong edge cooling either by gas puff, pellet injection or co-NBI heating in TEXTOR [10]. The turbulence rotation decreases during ECR heating. Such behavior may be naturally connected with the decrease of the radial electric field under ECRH.

9. Turbulence behavior in transient e-ITB after the end of off-axis ECRH

The recent T-10 experiment with off-axis ECRH showed that the amplitude of density fluctuation in the center during ECRH are higher in 2-3 times then in OH phase, in spite of low R/Lt=4 (Lt-temperature scale length). The modeling with ASTRA code reveals the high influx of the neutrals to the plasma center. This is in good correlation with the strong increase of LF QC, which typically associated with high particles convection. Strong electron temperature gradient R/Lt=16 and local minimum of turbulence amplitude and

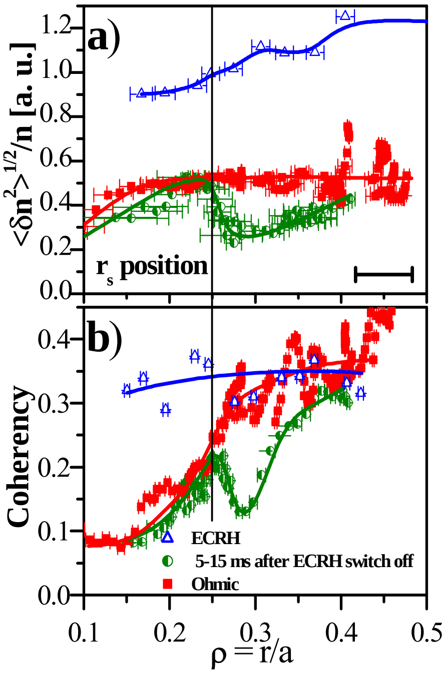

FIG. 16. Profiles of density fluctuations amplitude and poloidal coherency

coherency are observed at r/a ~ 0.3 15 ms after ECRH switch off. This proves e-ITB formation. The radial distribution of the turbulence amplitude and poloidal coherency is shown in Fig. 16. The measured constancy of the angular rotation excludes the mechanism of the turbulence suppression with velocity shear. One of the possible mechanism of ITB formation is the decrease of a number of rational surfaces near q=1 at low magnetic shear (see more in EX/P6-26).

10. Dynamic turbulence behavior

A non-local transport phenomena draw significant attention [17]. Figure 17 present the behavior of the central turbulence and SXR emission after edge cooling with Ne puff. Edge cooling leads to strong drop within 1 ms of HF QC turbulence at ρ=0.4, increase within 2 ms of the core SXR radiation and density peaking. Possible explanation of this phenomenon may be connected with the strong decrease of the edge rotation, causing temporal velocity shear between edge and core and suppression of QC turbulence due to velocity shear. Additional example of the strong turbulence dynamic variation was obtained in initial phase of central ECR heating, where the ohmic confinement maintains up to 20 ms. after the heating start and deteriorates only after increase of edge recycling. The phenomenon of the Delay of Confinement Deterioration was earlier observed in ASDEX [28] with NBI and in T-10 [29] with ECRH. The turbulence evolution during initial phase of central ECRH are shown in Fig. 18. In spite of the decrease

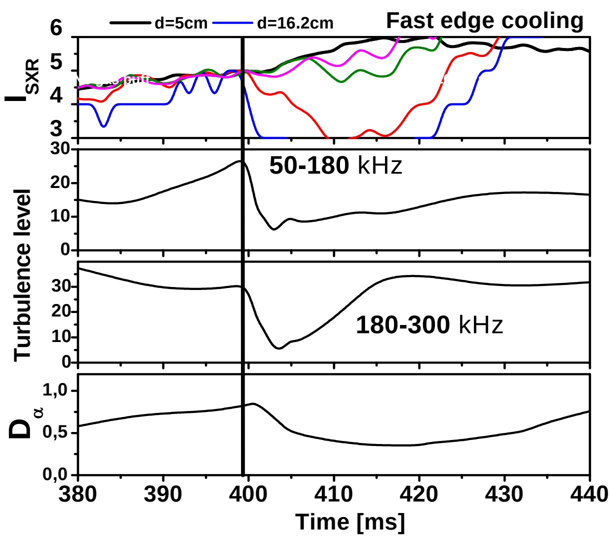

FIG. 17. Fast plasma edge cooling with carbon flake

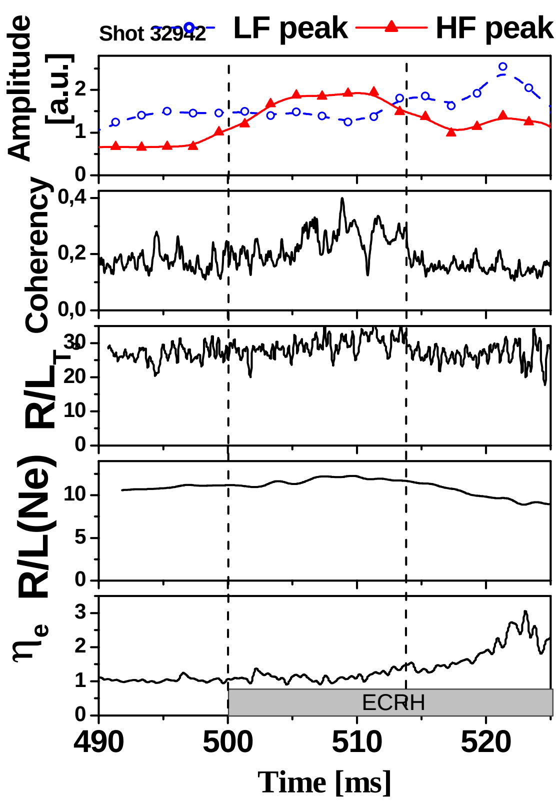

FIG. 18. Time traces of plasma characteristics during ECRH initial stage

of the coherent properties of turbulence in stationary ECRH, significant increase of coherency was observed during first 5 – 20 ms. of the heating. The coherency increase disappeared shortly after the increase of plasma interaction with the wall and corresponding strong rise of recycling at the edge and broadening of the density profile. The similar to SOC/IOC turbulence type transition was also observed. The high frequency QC turbulence dominates at the first 5 – 10 ms. It is gradually substituted by low frequency QC after beginning of density profile broadening. The excitation of TEM is natural during the initial electron temperature rise with unchanged peaked density. The subsequent transition to ITG after density profile broadening is also consistent with theory. Although the reflection layer for the data in Fig. 25 was at 20 cm., but additional experiments were carried out with reflection layer from 6 to 20 cm with the same result.

11. Conclusions

The experiments showed that the turbulence spectra retain the features of the linear instability in high OH confinement discharges. These features steadily vanish with the transition to strong non-linear regime with the increase of the heating power.The “Broad Band” turbulence with minimal radial scale arises due to stochastic excitation of a single high m mode, while “Quasi-Coherent” represent toroidal coupling of several modes. Experiment consistent with the existing of three different instabilities: in core - ITG (LF QC) and DTEM (HF QC); and Ballooning Resistive Interchange in SOL; LF QC (ITG) typically associated with the regions with high level of particles fluxes at plasma edge and low density, or with flat density gradient in center zone; HF QC (DTEM), in difference, typical for low particles fluxes region and high electron temperature gradients; OH and ECRH discharges showed the transition from LF to HF QC with increase of density from low up to critical. The integrate turbulence level not depends on n_e, despite change of the mode type. Turbulence level at half radius increases with total power; Special modes near 15 – 30 kHz were observed with properties of Geodesic Acoustic Mode, which is the branch of “zonal flows”. But its radial localization at rational surfaces contradicts to existing theories. The predicted “zonal flows” near zero frequency haven’t seen yet; QC oscillations tends to rotate as a rigid body with velocity of MHD m/n=2/1 island that suppose mechanism of long distance interaction between fluctuations at different radii and global MHD modes. This interaction could be destroyed by the relatively weak velocity shear (SOC-IOC, cold puff). Turbulence rotation significantly decreases during ECR heating. Significant progress was achieved both in experimental turbulence characterization and in theory, but, unfortunately, a few works exist up to now on their direct comparison. The future common work in this direction should clarify the turbulence physics and its impact on plasma transport.

This work was supported Nuclear Science and technology Department of Minatom RF, Scientific School 1608.2003.2, RFBR (Grant 04-02-17567), NWO 047.016.015 and INTAS (Gr. 2001 - 2056).

[1] V. A. Vershkov, et al, 21st EPS, 1994, Montpellier, France, V. 18 B, part III, p. 1192
[2] Vershkov V.A., et al, 15th IAEA Conf., Seville, 1994, Vol. 2, IAEA, Vienna (1995) 65.
[3] Vershkov V.A. et al, 16th IAEA Conf, Montreal, 1996, Vol. 1, IAEA, Vienna (1997) 519.
[4] Vershkov V.A., et al, Journal of Nuclear Matter., **241-243** (1997) 873.
[5] V.A. Vershkov et al, Nuclear Fusion (Yokohama Special Issue 2), **39** (1999) 1775.
[6] V.A. Vershkov *et al* RSI, 1999, V. 70, N. 3, p. 2903.
[7] V.A. Vershkov et al, 19 IAEA Fus. Energy Conf., Lyon, France, 2002, CN-94/EX/P3-04
[8] A.V. Melnikov et al, 30 EPS, St. Petersburg, Russia (2003) ECA Vol. 27A, P-3.114.

[9] M.V. Osipenko, Nuclear Fusion, **43**, (2003) 1641
[10] Vershkov V, et al, 31 EPS Conf., London, UK, 2004, O2_06
[11] J. Weiland, H. Horton, Nuclear Fusion, **31**,(1991) 390
[12] B.B. Kadomtsev, O.P. Pogutse, Rev. Plasma Phys., Vol. 5, Chapter 2
[13] M.V. Osipenko, Nuclear Fusion, **43**, (2003) 1641.
[14] Greenfield *et al*, Phys Plasmas **4** 1596 (1997)
[15] A. D. Beklemishev, W. Horton, Phys Fluids B 4 (1), 1992
[16] C. Bourdelle *et al*, Phys Plasmas **10** 2881 (2003)
[17] K. W. Gentle, et al, Phys. Rev. Lett, **74**, (1995) 3620
[18] K.N.Klimov et al., Proceedings of 2000 International Conference on Mathematical Methods in Electrodynamic Theory, Vol 1, Kharkov, Ukraine, 2000, p 128
[19] R. E. Walts *et al* Phys. Plasmas **1**, 2229, (1994)
[20] G. Manfredi et al, Plasma Phys. Contr. Fusion, **43**, (2001) 825-837.
[21] H. Y. Tsui, et al, Phys. Fluids B 5 (4) 1993, p. 1274.
[22] G. R. McKee, et al, Physics of Plasmas, **10** ,(2003) 1712
[23] A. Fujisawa, 31 EPS Conf., London, UK, 2004, O2_04
[24] G. Conway, 31 EPS Conf., London, UK, 2004, P4_124
[25] T.S.Hahm, et al., Phys. Plasmas **6**, 922, (1999).
[26] N. Winsor, et al, Phys. Fluids, **11**, (1968) 2448
[27] S.V. Soldatov et al, Proc. 24 EPS,, Berchtesgarden (1997), Vol. 21A, Part 2, p. 673.
[28] G. Fussman *et al* Proc. 12 IAEA Conf., Nice, 1988, V.1, IAEA, Vienna (1989) 145.
[29] A. V. Sushkov, et al, 17 EPS, Amsterdam, Holland(1990) V. 14 B, Part III, p. 1076